Proceedings

Integral Sliding Mode Backstepping Control of an Asymmetric Electro-Hydrostatic Actuator Based on Extended State Observer [†]

Shuzhong Zhang [1],*, Su Li [1] and Fuquan Dai [1,2]

[1] School of Mechanical and Automotive Engineering, Fujian University of Technology, Fuzhou 350118, China; lisu4751@gmail.com (S.L.); fuquan_dai@163.com (F.D.)

[2] Fujian Haiyuan Composite Materials Technology Co., Ltd., Fuzhou 350002, China

* Correspondence: shuzhong_zhang@outlook.com; Tel.: +86-591-228-63232

[†] Presented at the First International Electronic Conference on Actuator Technology: Materials, Devices and Applications, 23–27 November 2020; Available online: https://iecat2020.sciforum.net/.

Abstract: To provide high output force and to reduce the installation space, the electro-hydrostatic actuator (EHA) usually adopts asymmetric cylinder. However, comprehensive effects produced by its asymmetric flow, parameter uncertainties and unknown disturbance make it difficult to achieve high-accuracy position control. This paper proposed an integral sliding mode backstepping control (ISMBC) based on extended state observer for the asymmetric EHA. Firstly, the principle of the EHA was analyzed and an EHA model was built. Furthermore, the state space equation of the EHA was established based on flow distribution analysis. Two extended state observers (ESO) were designed to achieve real-time estimation of the unmeasured system states, unmatched and matched disturbances. The backstepping method was used to compensate the matched and unmatched disturbance, and an integrated sliding mode controller was developed to eliminate the static error and to improve the response ability. Theoretical analysis indicates that the controller can guarantee the desired tracking performance for the actuator under time-varying unmatched disturbances, and can make the tracking error asymptotically converge to zero under constant matched disturbances. Finally, simulations were performed with the designed controller, backstepping controller and proportional–integral–derivative (PID) controller, respectively. Thereafter, detailed comparisons of the control performances were provided. The results show that the proposed controller can achieve better position tracking and stronger robustness in parameter changing compared with the backstepping controller and PID controller.

Keywords: asymmetric cylinder; electro-hydrostatic actuator (EHA); extended state observer (ESO); integral sliding mode backstepping control (ISMBC); position control

1. Introduction

Electro-hydrostatic actuators (EHAs) are widely used in aviation, shipbuilding, automobile and other industrial fields due to their small size, light weight, high efficiency and great reliability [1–3]. The EHA is a highly integrated direct driven hydraulic system that integrates an electric motor, a pump, an actuator, a tank, etc. [1,4]. It achieves variable power transmission of actuators by changing the rotation speed or the displacement of the pump [5]. Compared with the traditional valve-controlled system, the EHA eliminates the throttling loss caused by the multi-way valve and the overflow loss caused by the centralized oil supplies, which significantly improves the system efficiency [6,7].

Over the past 20 years, EHAs have been applied in high-precision industries such as aviation and submarines [8,9], but only adopting actuators with symmetrical structures. However, industrial

applications usually require asymmetric hydraulic actuators, having the advantages of smaller volume and larger output force [10]. The unbalanced flow in asymmetric EHAs, caused by the unequal effective cross-section areas in two chambers, seriously affects the control accuracy and dynamic response [11,12].

To solve this problem, many novel methods were proposed such as the development of asymmetric flow distribution pumps [13], the research of pump-valve-coordinated system [14] and the use of dual-pumps control system [15], and on the other hand, advanced control algorithms such as robust adaptive control [16–18], backstepping control and sliding mode control.

In addition, EHA has the characteristics of nonlinearities, parametric uncertainties and external disturbances [19–21]. These nonlinearities include fluid compressibility, nonlinear friction, internal and external leakage [22]. Parametric uncertainties are mainly caused by model inaccuracy and system parameters variation. The external disturbances mainly consist of the variation of external load force and unmodeled load force. The nonlinear friction reduces the response speed by affecting the transient characteristics of the EHA and leads to viscous and crawling phenomena in low-speed operation. Leakage in the EHA decreases steady-state accuracy. Parametric uncertainties normally require a high gain to improve the robustness of the system, which easily lead to over-design. External disturbances reduce system stability by influencing system output [23].

To solve these problems of nonlinearities, uncertainties and external disturbances, a lot of research has been conducted. Lin [24] regarded the nonlinear friction force as norm-bounded uncertainties, and developed a robust discrete-time sliding-mode control (DT-SMC) for an EHA system. Fu [25] applied neural networks to identify uncertainties online, combined RBF neural networks with fast terminal sliding mode controller, which not only solved the problem of sliding mode control depending on system parameters but also suppressed oscillation to some extent. Alemu [26] applied the extended state observer (ESO) to estimate the system states, uncertainties and external disturbances, used the friction model to compensate the friction force, and designed a sliding mode controller for the system, which improved the robustness while ensuring the tracking performance. Sun [27] developed a nonlinear robust motion controller based on the extended disturbance observer to compensate the estimation error of the outer position tracking loop, while the inner pressure control loop adopted a backstepping method to achieve accurate force control. Wang [28] introduced a feedback backstepping control algorithm based on the backstepping control theory for the high-order model of the EHA system to convert the complex nonlinear system into a linear system. Yang [29] introduced a filtered error function, and integrated a novel expected compensation adaptive control framework into the controller to reduce environmental noise. Shen [30] decomposed the 5th-order EHA dynamic model into four subsystems, and designed adaptive control laws, respectively, to solve the controller design problem of the high-order system. Yang [31] designed a linear state observer and a nonlinear disturbance observer to estimate the matched and unmatched disturbances in the system, and employed a continuously differentiable friction model to compensate the friction force.

The above research shows that combining the observer with advanced control theory is an effective method to solve the problems of nonlinearities, uncertainties and disturbances in hydraulic systems. Most scholars focus on improving the control performance of symmetric EHAs and valve-controlled systems. Therefore, this paper proposed a novel control strategy to solve the uncertainty problem of an asymmetric EHA. The electric motor speed control system was regarded as a separate module, and PI controller was adopted. The state equation of the asymmetric EHA system was established considering nonlinear friction, parameter uncertainty and external disturbance. The Stribeck static friction force model was used to identify the friction force; the unmodeled friction force was regarded as an external disturbance. The state equation was used to judge whether the disturbance and the control law were on the same channel. The disturbances were divided into matched disturbance and unmatched disturbance, two ESOs were established for estimation. The integral sliding mode algorithm was added in the first step of the backstepping design to reduce the steady-state error and to improve the robustness of the EHA. Based on the Lyapunov theory, the

stability and effectiveness of this control method were proven. The simulation results show that the controller has good steady-state characteristics and high control accuracy.

The remainder of this paper is organized as follows. Section 2 presents the principal analysis and model building of an asymmetric EHA. In Section 3, two ESOs are designed to deal with the disturbances and its convergence is verified. In Section 4, the integral sliding mode backstepping control (ISMBC) controller is proposed, and its stability is proven. Section 5 gives comparative simulation results. Finally, the conclusion is given in Section 6.

2. Principal Analysis and Modelling

2.1. Load Force Analysis of a Micro Crane

In this case study, the research object is the micro crane, as shown in Figure 1. The dimensions of the micro-crane were measured, and its 3D model was created in Solidworks. After that, the dynamic model of the crane was built by exporting a CAD assembly from Solidworks and importing into Matlab/Simulink. The output force of the EHA system installed on the crane mainly depends on the torque, angular acceleration.
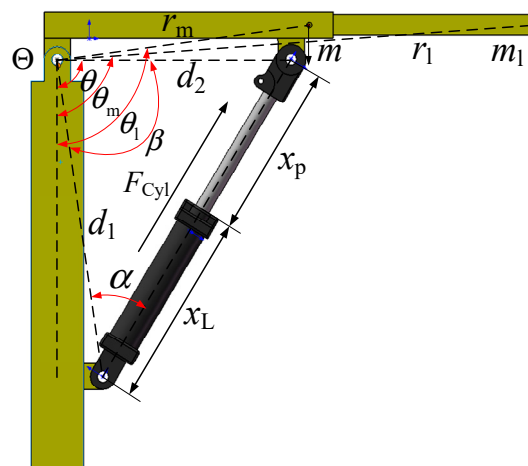

Figure 1. Structure diagram of the micro-crane.

According to Newton's second law, the torque balance equation of the boom can be written as:

$$\sum M_{\Theta} = J\frac{d^2\theta}{dt^2}, \tag{1}$$

where $d^2\theta/dt^2$ is the angular acceleration; J is the rotational inertia of boom.

Decomposed Equation (1) to obtain the output force equation of the hydraulic cylinder [15]

$$F_{\text{Cyl}} = \left[J\frac{d^2\theta}{dt^2} + mg \cdot r_m \sin(\theta_m) + m_l g \cdot r_l \sin(\theta_l)\right]\Big/d_1 \sin(\alpha), \tag{2}$$

where F_{Cyl} is the output force of cylinder; m is the mass of boom; r_m is the distance between the centre of mass and the joint; θ_m is the angle between the centre of mass and the reference coordinate vertical axis; g is gravitational acceleration; the load is connected to the crane by a hook and chain, and therefore, the load force is always perpendicular to the ground, such that m_l can be defined as load mass including the mass of load, hook and the chain; r_l is the distance from the load acting on the arm to the joint; θ_l is the angle between the connection about the joint and load with the reference coordinate vertical axis; d_1 is the distance between the cylinder base and the joint; α is the angle between the cylinder and the joint.

Next, the working principle of asymmetric EHA was analyzed, and the state-space equation was established for the EHA.

2.2. Principle Analysis of EHA

The schematic of the EHA control system is shown in Figure 2. The system includes the hydraulic system, the electric motor and the controller. The variable speed electric motor is controlled by PI controller, which drives a bidirectional fixed pump. Two pilot-operated check valves are used to balance the flow of the asymmetric cylinder. Two relief valves are used for safety purposes.
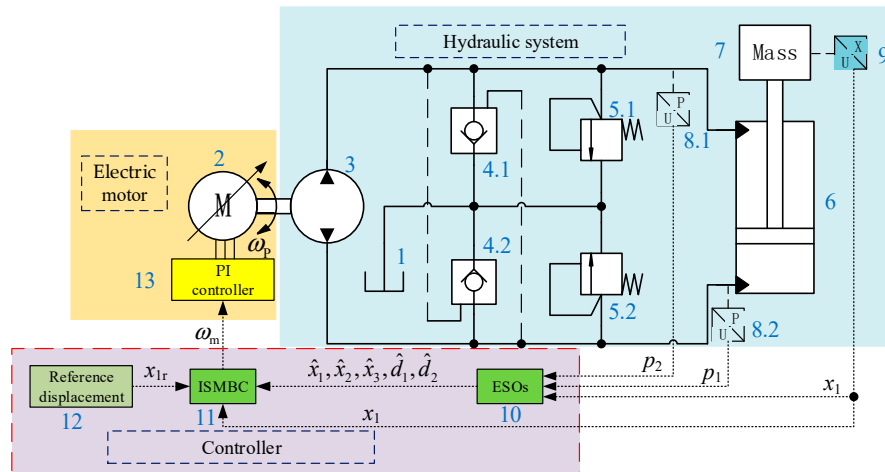

Figure 2. Schematic diagram of an asymmetric electro-hydrostatic actuator (EHA).

The EHA, installed on the micro-crane as shown in Figure 1, runs in two operating conditions including extending and retracting with positive load, as shown in Figure 3. Therefore, the load pressure p_L is always greater than zero; this was given by

$$p_L = p_1 - ap_2. \tag{3}$$

where p_1 and p_2 are the pressures of the piston chamber and the rod chamber of the cylinder, respectively; a is the area ratio of cylinder, $a = A_2/A_1$; A_1 and A_2 are the areas of the piston chamber and the rod chamber of the cylinder, m².
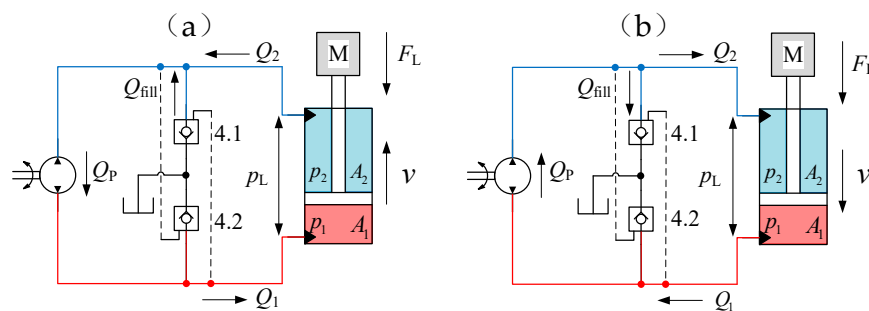

Figure 3. Schematic diagram of two operating conditions of EHA: (**a**) the EHA resistive extension; (**b**) the EHA assistive retraction.

Due to the different effective areas of the asymmetric cylinder, EHA requires unequal oil flow rate during moving. To prevent cavitation, hydraulic oil is replenished from the oil tank through the pilot-operated check valve 4.1, as shown in Figure 3a. During retracting, the excess oil flow from the piston chamber backs to the oil tank through the pilot-operated check valve 4.1, as shown in Figure 3b.

2.3. Modelling

2.3.1. Model of the Electric Motor

Permanent magnet synchronous motors (PMSMs) are widely used in industrial equipment because of high power density, high efficiency and high reliability. Hence, in this paper, a PMSM was selected to drive the EHA. The electromagnetic torque equation of PMSM in *d-q* reference frame can be expressed as

$$T_E = 1.5 p_n \psi_m i_{sq}, \tag{4}$$

where T_E is the electromagnetic torque; p_n is the number of pole pairs; ψ_m is the rotor magnet flux linkage; i_{sq} is the q-axis stator currents.

Assuming the PMSM rotates at a constant speed, the torque balance equation between the PMSM and the pump can be written as

$$\dot{\omega}_m = \frac{1}{J}\left(1.5 p_n \psi_m i_{sq} - B\omega_m - T_L\right), \tag{5}$$

where J is the moment of inertia; B is the viscous friction coefficient; T_L is the load torque from the pump; ω_m is the angular speed of the rotor.

In the Laplace transformation of Equation (5), ignoring the effects of the pump torque, the transfer function of the motor can be given as

$$\frac{\omega_m(s)}{I_{sq}(s)} = \frac{K}{\tau s - 1}. \tag{6}$$

where K is the electric motor gain, $K = 1.5 p_n \psi_m / B$; τ is the time constant, $\tau = J/B$.

The PMSM mainly adopts $i_{sd} = 0$ vector control; the outer loop speed control provides a reference signal for the inner current loop. This paper focuses on designing high-precision EHA system controller, so the proportional-integral (PI) was used as a speed loop controller for the electric motor.

2.3.2. Model of the Hydraulic System

The output flow of the pump can expressed by

$$Q_P = \frac{D_P}{2\pi}\omega_P - c_i \Delta p, \tag{7}$$

where Q_P is the output flow of pump, m³/s; D_P is the pump displacement, m³/r; ω_P is the pump angular speed, $\omega_P = \omega_m$, rad/s; c_i is the internal leakage coefficient, (m/s)/Pa; Δp is the differential pressure, $\Delta p = p_1 - p_2$.

Due to the pressure p_2 close to zero, for simplification, assuming $\Delta p \approx p_L$, Equation (7) can be rewritten as

$$Q_P = \frac{D_P}{2\pi}\omega_P - c_i p_L. \tag{8}$$

The flow-pressure equation of cylinder can be expressed as

$$\begin{cases} Q_P = Q_1 = A_1 \dot{x}_P + V_1 \dot{p}_1/\beta_e \\ -aQ_P = Q_2 = A_2 \dot{x}_P + V_2 \dot{p}_2/\beta_e \end{cases}, \tag{9}$$

where Q_1 and Q_2 are flowrates of the piston chamber and the rod chamber of the cylinder, m³/s; β_e is the effective bulk modulus, Pa; V_1 and V_2 are the current volumes of the cylinder, m³, $V_1 = V_{01} + A_1 x_P$, $V_2 = V_{02} - A_2(s - x_P)$; V_{01} and V_{02} are the initial volumes of two-chambers of the cylinder; s is the piston stroke, m.

Assuming that the piston is moving around the centre position, the following approximation can be given [32]:

$$\frac{V_1}{\beta_e} \approx \frac{V_2}{\beta_e} \approx \frac{V_{01}+V_{02}}{2\beta_e} = \frac{V_t}{2\beta_e}, \tag{10}$$

where V_t defines the total volume of the hydraulic cylinder, m³.

Combining Equations (7)–(10), the following equation can be obtained:

$$\frac{V_t}{2\beta_e}\dot{p}_L = \frac{\kappa D_P}{2\pi}\omega_P - \kappa c_i p_L - \kappa A_1 \dot{x}_P, \tag{11}$$

where $\kappa = 1 + a^2$.

The force balance equation of the hydraulic cylinder can be written as:

$$m\ddot{x}_P = A_1 p_L - F_f(\dot{x}_P) - F_L - d_t, \tag{12}$$

where m is the total load mass of the crane; F_L is the load force; d_t represents unmodeled friction, load force and external disturbance; $F_f(\dot{x}_P)$ denotes the Stribeck friction force and its model can be given by:

$$F_f(\dot{x}_P) = \left(F_C + (F_{brk} - F_C) \cdot e^{(-c_v|v|)}\right) sgn(v) + fv, |v| \geq v_{th},$$

$$F_f(\dot{x}_P) = v\frac{\left(fv_{th} + \left(F_C + (F_{brk} - F_C) \cdot e^{(-c_v|v|)}\right)\right)}{v_{th}}, |v| < v_{th}, \tag{13}$$

where F_C and F_{brk} are the coulomb friction and breakaway friction; c_v is the speed coefficient; v is the speed of the piston, $v = \dot{x}_P$; f is the viscous friction coefficient; v_{th} is the critical speed.

Combining Equations (11) and (12), defining state variables $x = [x_1, x_2, x_3] = [x_P, \dot{x}_P, p_L]$, the state-space equation of the EHA can be written as:

$$\begin{cases} \dot{x}_1 = x_2 \\ \dot{x}_2 = \theta_1 x_3 - \theta_2 F_f(x_2) - \theta_2 F_L - \theta_2 d_t \\ \dot{x}_3 = bu_\omega - \theta_3 x_2 - \theta_4 x_3 \\ y = x_1 \end{cases}, \tag{14}$$

For simplification, the parameters set can be denoted as $\theta_1 = \frac{A_1}{m}$, $\theta_2 = \frac{1}{m}$, $\theta_3 = \frac{2\kappa\beta_e A_1}{V_t}$, $\theta_4 = \frac{2\kappa\beta_e c_i}{V_t}$, $b = \frac{\kappa\beta_e D_P}{\pi V_t}$. Since the external load force and external disturbance cannot be directly measured, two ESOs are designed to estimate them later. To facilitate the design of the observer, the load force and external disturbance are combined into one item, $d_1(t) = -\theta_2 F_L - \theta_2 d_t$. Due to the wear, the change of temperature and pressure in the hydraulic system, parameters β_e, f, c_i, V_t, etc., become uncertain, which will cause internal disturbance, $d_2(t) = \Delta bu_\omega - \Delta\theta_3 x_2 - \Delta\theta_4 x_3$. Therefore, Equation (14) can be rewritten as:

$$\begin{cases} \dot{x}_1 = x_2 \\ \dot{x}_2 = \theta_1 x_3 - \theta_2 F_f(x_2) + d_1(t) \\ \dot{x}_3 = bu_\omega - \theta_3 x_2 - \theta_4 x_3 + d_2(t) \\ y = x_1 \end{cases}. \tag{15}$$

Usually, $d_1(t)$ is regarded as the unmatched disturbance, while $d_2(t)$ is considered as the matched disturbance. Because $d_2(t)$ and the control law u_ω are in the same channel, but $d_1(t)$ is in another channel, it cannot be eliminated directly by the control law.

Next, the integral sliding mode backstepping controller is designed to compensate for the matched disturbances and unmatched disturbances, to guarantee the cylinder actuator following smooth trajectory $y_d = x_{1d}$.

The following assumptions are necessary for the controller design.

Assumption 1. *The second-order time derivatives of tracking trajectory x_{1d}, and $\dot{x}_{1d}$, $\ddot{x}_{1d}$ are all bounded.*

Assumption 2. *The first-order time derivatives of disturbances $d_1(t)$ and $d_2(t)$, are all bounded by $|\dot{d}_1(t)| \leq \xi_1$, $|\dot{d}_2(t)| \leq \xi_2$. The positive constants ξ_1 and ξ_2 are all satisfied by $\xi_1, \xi_2 > 0$.*

Assumption 3. *The nonlinear term $F_f(x_2)$ is globally Lipschitz with respect to x_2, where $|\tilde{F}_f(x_2)| = |F_f(x_2) - F_f(\hat{x}_2)| \leq \tau|x_2 - \hat{x}_2|$, τ is the positive Lipschitz constant [33].*

3. Design and Analysis of ESOs

3.1. Design of ESOs

The traditional state observer can only be used to observe unknown state variables in the system, such as position x_P, velocity $\dot{x}_P$ and load pressure p_L. However, the unmatched disturbance and the matched disturbance cannot be effectively estimated. In this paper, the system model (15) of the EHA was divided into a position–velocity subsystem and a pressure subsystem. The disturbances $d_1(t)$ and $d_2(t)$ were extended, respectively. Two ESOs were designed to estimate the unmatched disturbance and the matched disturbance in real-time, respectively. The position–velocity subsystem is expressed as:

$$\begin{cases} \dot{x}_1 = x_2 \\ \dot{x}_2 = \theta_1 x_3 - \theta_2 F_f(x_2) + x_{e1} \\ \dot{x}_{e1} = w_1 \\ y_1 = x_1 \end{cases}, \tag{16}$$

where y_1 is the output of the position–velocity subsystem, $x_{e1} = d_1(t)$, $\dot{x}_{e1} = \dot{d}_1(t) = w_1$.

The pressure subsystem can be expressed as:

$$\begin{cases} \dot{x}_3 = bu_\omega - \theta_3 x_2 - \theta_4 x_3 + x_{e2} \\ \dot{x}_{e2} = w_2 \\ y_2 = x_3 \end{cases}, \tag{17}$$

where y_1 is the output of the pressure subsystem, $x_{e2} = d_2(t)$, $\dot{x}_{e2} = \dot{d}_2(t) = w_2$.

Two ESOs for two subsystems are given as:

$$\begin{cases} \dot{\hat{x}}_1 = \hat{x}_2 + l_1(x_1 - \hat{x}_1) \\ \dot{\hat{x}}_2 = \theta_1 \hat{x}_3 - \theta_2 F_f(\hat{x}_2) + \hat{x}_{e1} + l_2(x_1 - \hat{x}_1) \\ \dot{\hat{x}}_{e1} = l_3(x_1 - \hat{x}_1) \end{cases}, \tag{18}$$

$$\begin{cases} \dot{\hat{x}}_3 = bu_\omega - \theta_3 \hat{x}_2 - \theta_4 \hat{x}_3 + \hat{x}_{e2} + h_1(x_3 - \hat{x}_3) \\ \dot{\hat{x}}_{e2} = h_2(x_3 - \hat{x}_3) \end{cases}, \tag{19}$$

where $\hat{*}$ represents the estimation value of $*$; the observer gains $L = [l_1, l_2, l_3] = [3w_o, 3w_o^2, w_o^3]$, $H = [h_1, h_2] = [2w_c, w_c^2]$. Furthermore, the estimation error is defined as $\tilde{*} = * - \hat{*}$ and is represented as:

$$\begin{cases} \dot{\tilde{x}}_1 = -3w_o\tilde{x}_1 + \tilde{x}_2 \\ \dot{\tilde{x}}_2 = -3w_o^2\tilde{x}_1 + \theta_1\tilde{x}_3 - \theta_2\tilde{F}_f + \hat{x}_{e1}, \\ \dot{\hat{x}}_{e1} = -w_o^3\tilde{x}_1 + w_1 \end{cases} \tag{20}$$

$$\begin{cases} \dot{\tilde{x}}_3 = -2w_c^2\tilde{x}_3 - \theta_3\tilde{x}_2 - \theta_4\tilde{x}_3 + \tilde{x}_{e2} \\ \dot{\tilde{x}}_{e2} = -w_c^2\tilde{x}_3 + w_2 \end{cases}, \tag{21}$$

Remark 1. *The model* $F_f(\hat{x}_2)$ *represents the estimation of the nonlinear friction force, which can be obtained by substituting the observation value* $\hat{x}_2$ *into* $F_f(x_2)$. $\tilde{F}_f$ *is defined as the estimation error of the friction force,* $\tilde{F}_f = F_f(x_2) - F_f(\hat{x}_2)$.

Then, the scaled estimation errors are defined as $\varepsilon = [\varepsilon_1, \varepsilon_2, \varepsilon_3] = [\tilde{x}_1, \tilde{x}_2/w_o, \tilde{x}_{e1}/w_o^2]$ in the position–velocity subsystem and $\epsilon = [\epsilon_1, \epsilon_2] = [\tilde{x}_3, \tilde{x}_{e2}/w_c]$ in the pressure subsystem. Therefore, the dynamics of the scaled estimation errors can be described as:

$$\dot{\varepsilon} = w_o A_\varepsilon \varepsilon + B_{\varepsilon 1}\frac{\theta_1\tilde{x}_3 - \theta_2\tilde{F}_f}{w_o} + B_{\varepsilon 2}\frac{w_1}{w_o^2}, \tag{22}$$

$$\dot{\epsilon} = w_c A_\epsilon \epsilon + B_{\epsilon 1}\frac{-\theta_3\tilde{x}_2}{w_c} + B_{\epsilon 2}\frac{w_2}{w_c}, \tag{23}$$

where $A_\varepsilon = \begin{bmatrix} -3 & 1 & 0 \\ -3 & 0 & 1 \\ -1 & 0 & 0 \end{bmatrix}$, $B_{\varepsilon 1} = \begin{bmatrix} 0 \\ 1 \\ 0 \end{bmatrix}$, $B_{\varepsilon 2} = \begin{bmatrix} 0 \\ 0 \\ 1 \end{bmatrix}$, $A_\epsilon = \begin{bmatrix} -2 - \theta_4 & 1 \\ -1 & 0 \end{bmatrix}$, $B_{\epsilon 1} = \begin{bmatrix} 1 \\ 0 \end{bmatrix}$, $B_{\epsilon 2} = \begin{bmatrix} 0 \\ 1 \end{bmatrix}$.

As the matrix A_ε and A_ϵ is Hurwitz, two positive definite matrixs P_ε and P_ϵ hold the following matrix equality:

$$A_\varepsilon^T P_\varepsilon + P_\varepsilon A_\varepsilon = -I_1, \tag{24}$$

$$A_\epsilon^T P_\epsilon + P_\epsilon A_\epsilon = -I_2. \tag{25}$$

3.2. Lyapunov Analysis of ESOs

Based on Assumption 1 and Assumption 2, The ESO1 was designed to observe the unmatched disturbance and the velocity of the position–velocity subsystem, and the ESO2 was used to observe the matched disturbance, respectively. Next, in view of the Lyapunov method, the stability of the designed ESOs was analyzed. The analysis method was divided into two parts, corresponding to two ESOs.

Part 1: Stability analysis of the ESO1 that includes unknown state and unmatched disturbance.

Define the Lyapunov function V_1

$$V_1 = \varepsilon^T P_\varepsilon \varepsilon, \tag{26}$$

Combine Equations (22) and (24) and take the derivative of Equation (26), obtain:

$$\begin{aligned} \dot{V}_1 &= \dot{\varepsilon}^T P_\varepsilon \varepsilon + \varepsilon^T P_\varepsilon \dot{\varepsilon} \\ &= \varepsilon^T (A_\varepsilon^T P_\varepsilon + P_\varepsilon A_\varepsilon)\varepsilon + 2\varepsilon^T P_\varepsilon B_{\varepsilon 1}\left(\theta_1\tilde{x}_3 - \theta_2\tilde{F}_f\right)/w_o + 2\varepsilon^T P_\varepsilon B_{\varepsilon 2}\, w_1/w_o^2 \\ &= -\varepsilon^T I_1 \varepsilon + 2\varepsilon^T P_\varepsilon B_{\varepsilon 1}\left(\theta_1\tilde{x}_3 - \theta_2\tilde{F}_f\right)/w_o + 2\varepsilon^T P_\varepsilon B_{\varepsilon 2}\, w_1/w_o^2 \\ &\leq -\|\varepsilon\|\left(\lambda_{min}(I_1)\|\varepsilon\| - 2(\|P_\varepsilon B_{\varepsilon 1}\|\left(\theta_1\mu_3 - \theta_2\tau\mu_2\right)/w_o + \|P_\varepsilon B_{\varepsilon 2}\|\,\xi_1/w_o^2)\right) \\ &= -\|\varepsilon\|(\lambda_{min}(I_1)\|\varepsilon\| - 2\vartheta_1) \end{aligned} \tag{27}$$

where $\vartheta_1 = 2\left(\|P_\varepsilon B_{\varepsilon 1}\|\frac{\theta_1\mu_3 - \theta_2\tau\mu_2}{w_o} + \|P_\varepsilon B_{\varepsilon 2}\|\frac{\xi_1}{w_o^2}\right)$

To guarantee the convergence of the designed ESO1, the derivative of V_1 must satisfy $\dot{V}_1 \leq 0$, in the way $\|\varepsilon\| \geq \frac{\vartheta_1}{\lambda_{\min}(I)}$. Additionally, considering $\|\varepsilon\|$ is ultimately bounded by $\|\varepsilon\| \leq \frac{\vartheta_1}{\lambda_{\min}(I)}$. Then,

this means that $\tilde{x}_1$, $\tilde{x}_2$, $\tilde{x}_3$, $\tilde{x}_{e1}$ all exist boundaries. Thus, there must be a set of known positive constants μ_1, μ_2, μ_3 and μ_4 that satisfy $|\tilde{x}_1| \leq \mu_1$, $|\tilde{x}_2| \leq \mu_2$, $|\tilde{x}_3| \leq \mu_3$ and $|\tilde{x}_{e1}| \leq \mu_4$.

Part 2: Stability analysis of the ESO2 that contains matched disturbance.

Define the Lyapunov function V_2

$$V_2 = \epsilon^T P_\epsilon \epsilon. \tag{28}$$

Combine Equation (23) with (25) and take the derivative of Equation (28), obtain:

$$
\begin{aligned}
\dot{V}_2 &= \dot{\epsilon}^T P_\epsilon \epsilon + \epsilon^T P_\epsilon \dot{\epsilon} \\
&= \epsilon^T (A_\epsilon^T P_\epsilon + P_\epsilon A_\epsilon)\epsilon - 2\theta_3 \epsilon^T P_\epsilon B_{\epsilon 1} \tilde{x}_2/w_c + 2\epsilon^T P_\epsilon B_{\epsilon 2} w_2/w_c \\
&= -\epsilon^T I_2 \epsilon - 2\theta_3 \epsilon^T P_\epsilon B_{\epsilon 1} \tilde{x}_2/w_c + 2\epsilon^T P_\epsilon B_{\epsilon 2} w_2/w_c \\
&\leq -\lambda_{min}(I_2)\|\epsilon\|^2 + 2\|\epsilon\|\|P_\epsilon B_{\epsilon 1}\|\theta_3 \mu_2/w_c + 2\|\epsilon\|\|P_\epsilon B_{\epsilon 2}\|\mu_5/w_c \\
&= -\|\epsilon\|(\lambda_{min}(I_2)\|\epsilon\| - \vartheta_2)
\end{aligned}
\tag{29}
$$

where $\vartheta_2 = 2\|P_\epsilon B_{\epsilon 1}\|\theta_3 \mu_2/w_c + 2\|P_\epsilon B_{\epsilon 2}\|\mu_5/w_c$.

To ensure the convergence of the designed ESO2, the derivative of V_1 must satisfy $\dot{V}_1 \leq 0$, in the way $\|\epsilon\| \geq \frac{\vartheta_2}{\lambda_{\min}(I_2)}$. Always, consider that $\|\varepsilon\|$ is ultimately bounded by $\|\epsilon\| \leq \frac{\vartheta_2}{\lambda_{\min}(I_2)}$. Then, it means that $\tilde{x}_{e1}$ exists a boundary. There must be a known positive constant μ_5 that satisfies $|\tilde{x}_{e2}| \leq \mu_5$.

4. Design and Analysis of ISMBC Controller

4.1. Design of the Controller

In this paper, the backstepping design was applied to compensate for the disturbances of matched items and unmatched items in the EHA. In order to further reduce the tracking error and suppress the oscillation of the EHA, an integral sliding mode control algorithm is introduced into the position control term.

According to the system (15), it can be known that the system feedback output y is the state x_1, and the tracking trajectory is defined as $y_d = x_{1d}$. Hence, the position tracking error e_1 of the EHA can be represented as

$$e_1 = x_1 - x_{1d}. \tag{30}$$

Using the system (15), the derivative equation of the tracking error e_1 can be expressed as:

$$\dot{e}_1 = x_2 - \dot{x}_{1d}. \tag{31}$$

Here, the sliding mode surface s is designed to ensure position tracking accuracy; an integral item is introduced to suppress the switching oscillation

$$s = e_1 + k_0 \zeta, \tag{32}$$

where ζ is the integral item, $\zeta = \int_0^t e_1 \, dt$; k_0 the integral gain that is a positive constant.

The derivative of the sliding surface s can be defined as:

$$\dot{s} = x_2 - \dot{x}_{1d} + k_0 e_1. \tag{33}$$

Select constant velocity approach law as the control law of integral sliding mode control

$$\dot{s} = -\rho sgn(s), \tag{34}$$

where ρ is the switching gain.

For the first equation of the system (15), in which the input is the state x_2. Due to that fact that x_2 cannot be obtained directly, a virtual control law a_1 is designed for x_2. The error function e_2 is defined as:

$$e_2 = x_2 - a_1, \tag{35}$$

Using Equation (33), the virtual control law a_1 can be designed as:

$$a_1 = \dot{x}_{1d} - k_1 s - k_0 e_1, \tag{36}$$

Combining Equations (33) and (36), the dynamic of the sliding surface s can be further expressed as:

$$\dot{s} = -k_1 s - \rho sgn(s) + e_2. \tag{37}$$

Therefore, the dynamic of the virtual control law a_1 can be represented as:

$$\dot{a}_1 = \ddot{x}_{1d} + k_1(k_1 + k_0)s - (k_1 + k_0)e_2 + k_0^2 e_1. \tag{38}$$

According to Equation (35), the error e_2 is unknown, since the state variable x_2 cannot be measured directly. Therefore, its estimated value $\hat{x}_2$ is introduced from the ESO1 (18); the virtual error e_2 can be split into two parts, including the computable part e_{2c} and the non-computable part e_{2u}

$$e_2 = e_{2c} + e_{2u}, e_{2c} = \hat{x}_2 - a_1, e_{2u} = x_2 - \hat{x}_2 = \tilde{x}_2. \tag{39}$$

Usually the computable part e_{2c} is used in the controller design. Based on Equations (15) and (35), the derivative of the virtual error e_2 can be written as:

$$\dot{e}_2 = \theta_1 x_3 - \theta_2 F_f(x_2) + d_1 - \dot{a}_1, \tag{40}$$

In this step, the state variable x_3 is used as the virtual control input. Then, a virtual control law a_2 is designed for it to improve tracking performance and to afford feed forward compensation for unmatched disturbances. Define virtual control input error e_3 as:

$$e_3 = x_3 - a_2. \tag{41}$$

The virtual control law a_2 can be designed as:

$$a_2 = \frac{1}{\theta_1}\left(\theta_2 F_f(\hat{x}_2) - \hat{d}_1 - s + \dot{a}_1 - k_2 e_2\right). \tag{42}$$

Combining Equations (40) with (42), the dynamic of the virtual error e_2 can be rewritten as:

$$\dot{e}_2 = \theta_1 e_3 - k_2 e_2 - \theta_2 \tilde{F}_f(x_2) + \tilde{d}_1 - s, \tag{43}$$

For the third equation of system (15), in which the input is u_ω, u_ω is also the control input of the EHA. According to the definition of a_2 and x_3, the virtual control error e_3 can be divided into a computable part e_{3c} and a non-computable part e_{3u}:

$$e_3 = e_{3c} + e_{3u}, e_{3c} = \hat{x}_3 - a_2, e_{3u} = x_3 - \hat{x}_3 = \tilde{x}_3. \tag{44}$$

Based on Equations (15) and (44), the derivative of the virtual error e_3 can be written as:

$$\dot{e}_3 = bu_\omega - \theta_3 x_2 - \theta_4 x_3 + d_2 - \dot{a}_2, \tag{45}$$

where $\dot{a}_2$ is defined as the dynamic of the virtual control law a_2, which can be calculated by:

$$\dot{a}_2 = \frac{1}{\theta_1}\left(\theta_2 \dot{F}_f(\hat{x}_2) - \dot{\hat{d}}_1 - \dot{s} + \ddot{a}_1 - k_2 \dot{e}_2\right),$$
$$\ddot{a}_1 = \ddot{x}_{1d} + k_1(k_1 + k_0)\dot{s} - (k_1 + k_0)\dot{e}_2 + k_0^2 \dot{e}_1, \tag{46}$$

where $\dot{F}_f(\hat{x}_2)$ is the dynamic of the estimate of friction, which can be obtained by a filter $\frac{Ns}{s+N}$, and N is the filter gain. $\dot{\hat{d}}_1$ is the dynamic of the estimate of unmatched disturbance, which can be obtained in the same way.

In view of the $\dot{e}_3$ approaching 0, the resulting control law u_ω is designed as

$$u_\omega = \frac{1}{b}\left(\theta_3 \hat{x}_2 + \theta_4 \hat{x}_3 - \hat{d}_2 + \dot{a}_2 - \theta_1 e_2 - k_2 e_{3c}\right), \tag{47}$$

Substituting the control law (47) into Equation (46), it follows that

$$\dot{e}_3 = -k_3 e_3 - \theta_1 e_2 - \theta_3 \tilde{x}_2 - \theta_4 \tilde{x}_3 + \tilde{d}_2. \tag{48}$$

4.2. Stability Analysis of the Controller

To prove the stability of the proposed ISMBC controller, the Lyapunov function of the controller is defined as V_3

$$V_3 = \tfrac{1}{2}s^2 + \tfrac{1}{2}e_2^2 + \tfrac{1}{2}e_3^2. \tag{49}$$

Consider the Lyapunov function of the total system as

$$V = V_1 + V_2 + V_3, \tag{50}$$

From Equation (27), one obtains

$$\begin{aligned}\dot{V}_1 &= -\varepsilon^T I_1 \varepsilon + 2\varepsilon^T P_\varepsilon B_{\varepsilon1}\left(\theta_1 \tilde{x}_3 - \theta_2 \tilde{F}_f\right)/w_o + 2\varepsilon^T P_\varepsilon B_{\varepsilon2}\, w_1/w_o^2, \\ &\leq -(\lambda_{min}(I_1) - 4)\|\varepsilon\|^2 + \Psi_1^2 \xi_1^2 + \Psi_2^2\|\varepsilon\|^2\end{aligned} \tag{51}$$

where $\Psi_1 = \frac{1}{w_o^2}\|P_\varepsilon B_{\varepsilon2}\|$, $\Psi_2 = \frac{\theta_1}{\omega_o}\|P_\varepsilon B_{\varepsilon1}\|$.

From Equation (29), one obtains

$$\begin{aligned}\dot{V}_2 &= -\epsilon^T I_2 \epsilon - 2\theta_3 \epsilon^T P_\epsilon B_{\epsilon1}\, \tilde{x}_2/w_c + 2\epsilon^T P_\epsilon B_{\epsilon2}\, w_2/w_c, \\ &\leq -(\lambda_{min}(I_2) - 2)\|\epsilon\|^2 + \Psi_3^2 \xi_2^2 + \Psi_4^2\|\epsilon\|^2\end{aligned} \tag{52}$$

where $\Psi_3 = \frac{1}{w_c^2}\|P_\epsilon B_{\epsilon2}\|$, $\Psi_4 = \frac{\theta_3}{w_c}\|P_\epsilon B_{\epsilon1}\|$.

Differentiating V_3 and combining Equations (37), (43) and (48), one obtains

$$\begin{aligned}\dot{V}_3 &= ss + e_2\dot{e}_2 + e_3\dot{e}_3 \\ &= s(-k_1 s - \rho sgn(s) + e_2) + e_2(\theta_1 e_3 - k_2 e_2 - \theta_2 \tilde{F}_f(x_2) + \tilde{d}_1 - s) + e_3(-k_3 e_3 - \theta_3 \tilde{x}_2 - \theta_4 \tilde{x}_3 + \tilde{d}_2) \\ &= -k_1 s^2 - k_2 e_2^2 - k_3 e_3^2 - \rho|s| - \theta_2 e_2 \tilde{F}_f(x_2) + e_2 \tilde{d}_1 - \theta_3 e_3 \tilde{x}_2 - \theta_4 e_3 \tilde{x}_3 + e_3 \tilde{d}_2 \\ &\leq -k_1 s^2 - \left(k_2 + \tfrac{1}{2}\theta_2\tau - \tfrac{1}{2}\right)e_2^2 - \left(k_3 + \tfrac{1}{2}\theta_3 + \tfrac{1}{2}\theta_4 - \tfrac{1}{2}\right)e_3^2 - \rho|s| + \Psi_5\|\varepsilon\|^2 + \Psi_6\|\epsilon\|^2\end{aligned} \tag{53}$$

where $\Psi_5 = \tfrac{1}{2}\min\{-\theta_2\tau - \theta_3, 1\}$, $\Psi_6 = \tfrac{1}{2}\min\{\theta_4, 1\}$.

Combining Equations (51), (52) and (53), the derivative of the Lyapunov function V is written as

$$\begin{aligned}\dot{V} &= \dot{V}_1 + \dot{V}_2 + \dot{V}_3 \\ &\leq -\varsigma_1\|\varepsilon\|^2 - \varsigma_2\|\epsilon\|^2 - \varsigma_3 s^2 - \varsigma_4 e_2^2 - \varsigma_5 e_3^2 - \varsigma_6|s| + \sigma'\end{aligned} \tag{54}$$

where $\varsigma_1 = \lambda_{min}(I_1) - 4 - \Psi_4^2 - \Psi_5$, $\varsigma_2 = \lambda_{min}(I_2) - 2 - \Psi_2^2 - \Psi_6$, $\varsigma_3 = k_1$, $\varsigma_4 = k_2 + \tfrac{1}{2}\theta_2\tau - \tfrac{1}{2}$, $\varsigma_5 = k_3 + \tfrac{1}{2}\theta_3 + \tfrac{1}{2}\theta_4 - \tfrac{1}{2}$, $\varsigma_6 = \rho$, $\sigma = -\rho|s| + \Psi_1^2 \xi_1^2 + \Psi_3^2 \xi_2^2$.

The necessary and sufficient conditions for the stability of the control system should satisfy

$$\dot{V} \leq 0 \tag{55}$$

From Equation (54), if condition (55) is satisfied, the following inequality holds by seleceting control parameters:

$$\begin{aligned}&\varsigma_i \geq 0, i = 1,2,\cdots,6 \\ &\varsigma_1\|\varepsilon\|^2 + \varsigma_2\|\epsilon\|^2 + \varsigma_3 s^2 + \varsigma_4 e_2^2 + \varsigma_5 e_3^2 + \varsigma_6|s| \geq \sigma'\end{aligned} \tag{56}$$

According to inequality (56) and omitting integral term s and sliding mode term $\rho|s|$, greater controller gain is required to achieve the control system stability. Therefore, it can be concluded that the introduction of integral sliding mode control into the backstepping design can achieve higher stability and better robustness.

5. Simulation Analysis

5.1. Simulation Model

To verify the control performance of the proposed controller, a multi-domain model was established in Matlab/Simulink, as shown in Figure 4. The simulation model considers the dynamic response of the motor, the uncertain factors in the hydraulic model including matched disturbance and unmatched disturbance. The parameters of the EHA are shown in Table 1. To prove the

superiority of the designed ISMBC controller, the following three control methods were used for comparison.

(1) Integral sliding mode backstepping control (ISMBC): this is the proposed control scheme in this paper, and the design is described in Section 4. The controller parameters were tuned by hand, $k_1 = 4500$; $k_2 = 100$; $k_3 = 3$; $k_0 = 30$; $w_0 = 1000$; $w_c = 5000$; $\rho = 0.5$.

(2) Backstepping control (BC): the control scheme is the same as the ISMBC controller but without integral sliding mode term. To verify the effectiveness of the integral sliding mode control method in the paper, let $c_0 = 0$ and $\rho = 0$. Other parameters are the same as those in the ISMBC controller.

(3) Proportional–integral–derivative control (PID): this is a classic control algorithm, which is widely used in industrial fields. This controller realizes the trajectory tracking by tuning the three parameters, including proportional gain k_P, integral gain k_i and derivative gain k_d. Properly increasing these gain parameters can improve the control accuracy, but the excessive gain would also cause oscillation and reduce system stability. Finally, through trial and error, parameters were set as: $k_P = 28500$; $k_i = 1000$; $k_d = 0$.
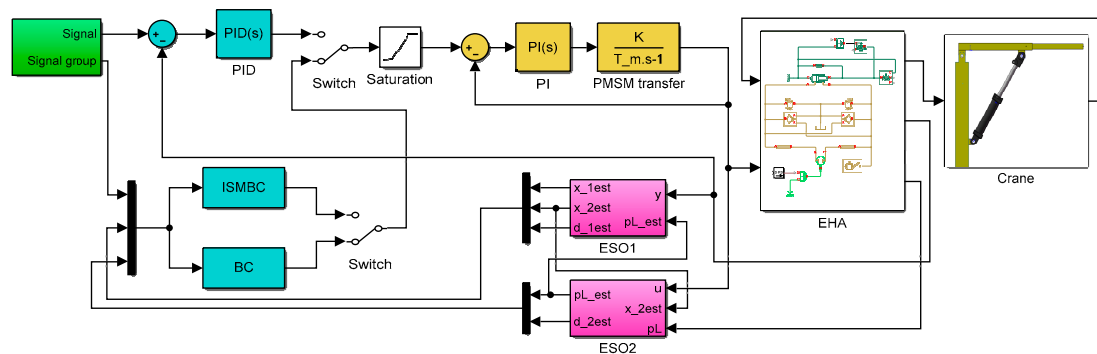

Figure 4. Schematic diagram of multi-domain model.

Table 1. Parameters of the EHA.

Parameter (unit)	Symbol	Value	Parameter (unit)	Symbol	Value
mass of boom (kg)	m	30	pump displacement (m³/r)	D_P	$13..3 \times 10^{-6}$
load mass (kg)	m_l	0–300	big chamber area (m²)	A_1	12.6×10^{-4}
gravitational acceleration (m/s²)	g	9.81	small chamber area (m²)	A_2	6.4×10^{-4}
motor gain (rad/(sA))	K	8.95	total volume (m³)	V_t	4.4×10^{-4}
motor time constant (s)	τ	7×10^4	cylinder stroke (m)	s	0.35
effective bulk modulus (Pa)	β_e	1.4×10^9	pump leakage coefficient ((m/s)/Pa)	c_i	2.93×10^9
critical speed (m/s)	v_{th}	10^{-4}	coulomb friction (N)	F_C	50
breakaway friction (N)	F_{brk}	100	viscous friction coefficient	f	2000
speed coefficient	c_v	10			

5.2. Results Analysis

5.2.1. Observer Verification

In view of the fact that the micro-crane mainly performs ascent and descent motions, the controller tracking trajectory was designed as a smooth curve with a max displacement of 0.3 m, starting to rise at t = 0.5 s, and starting to fall at t = 6 s. The desired position of the EHA is shown as the curve x_{1d} in Figure 5a.

Under the ISMBC controller, the actual output position of the EHA almost overlapped with the reference position signal. The maximum error occurred when the crane just started to descend; the

value was 0.124 mm; the EHA mean error was only 3.93×10^{-3} mm. It can be seen that the ISMBC controller can achieve high accuracy position control. On the other hand, the position estimation and position estimation error of the ESO1 are shown in Figure 5b. The maximum position estimation error was only 3.52×10^{-3} mm. The estimation error was small enough that the observed position can be regarded as the actual output position of the EHA. The estimated values of other state are shown in Figure 6. The observation results show that the designed dual-ESOs can provide accurate feedback values for ISMBC controller and BC controller.
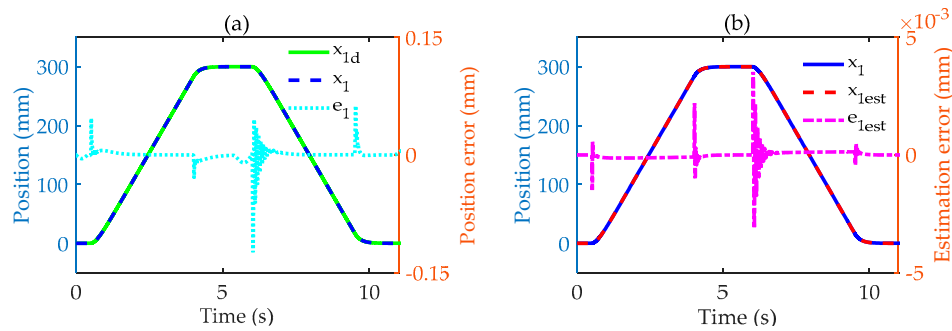

Figure 5. Tracking curve and estimation curve of hydraulic cylinder under integral sliding mode backstepping control (ISMBC): (**a**) position tracking and position error; (**b**) position estimation and position estimation error.
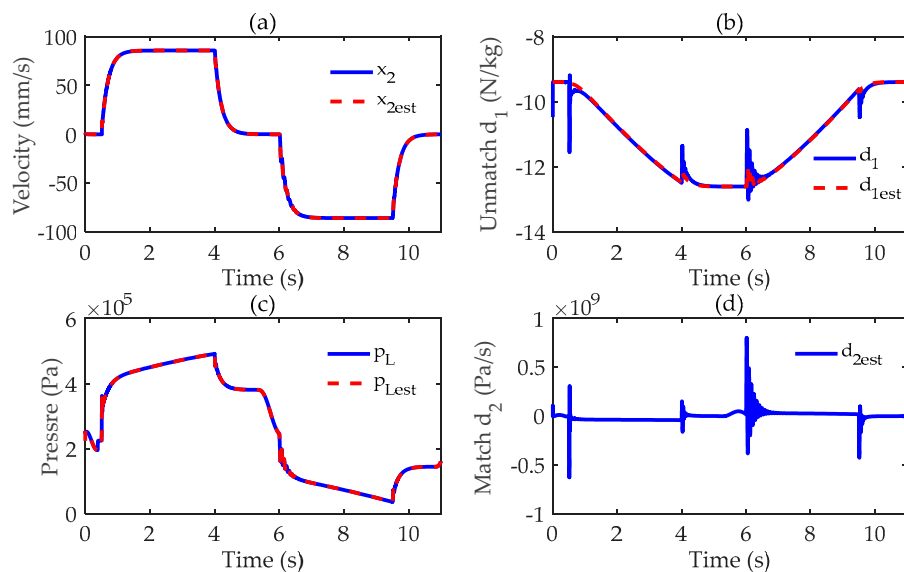

Figure 6. States and disturbances estimation of extended state observers (ESOs) under ISMBC controller: (**a**) velocity estimation; (**b**) unmatched disturbance estimation; (**c**) load pressure estimation; (**d**) matched disturbance estimation.

5.2.2. Control Performance without Load

Without load, the three controllers were used for the closed-loop position control of the EHA. The position error and control output of the three controllers are shown in Figure 7a,b, respectively. From Figure 7a, it can be seen that ISMBC possessed the highest control accuracy, and the position tracking error was almost approaching to zero; BC control accuracy was second to ISMBC, which shows that the integral sliding mode surface has the effect of reducing the tracking error. Meanwhile, if PID control is used to achieve higher control accuracy, the proportional gain must be increased, which would cause more severe oscillations to the system. In Figure 7b, the control output curves of the three controllers also prove this point. When the motor speed changes rapidly, the PID control

output will oscillate violently, which brings unstable factors to the system. The control output of ISMBC controller and BC controller is smoother.
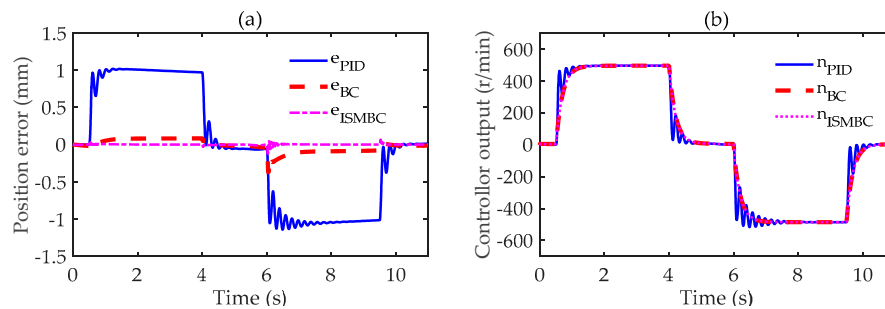

Figure 7. The comparison of control performance of the three controllers without load: (**a**) position tracking error; (**b**) controller output.

To intuitively express the control accuracy and stability of each controller, five evaluation indexes were defined to evaluate the performance of the control. Those indexes include maximum tracking error M_e, average tracking error μ_e, standard deviation of the tracking error σ_e average controller output μ_u and standard deviation of the controller output σ_u. Without load, the evaluation indexes of the three controllers are listed in Table 2. It can be seen that, except for σ_u, the ISMBC controller had the lowest indexes, so its control performance was the best, followed by BC controller, and the PID control performance was the worst.

Table 2. Comparison of evaluation indexes of the three controllers without load.

Controller	M_e [mm]	μ_e [mm]	σ_e [mm]	μ_u [mm]	σ_u [mm]
PID	1.14	7.17×10^{-2}	0.629	43.28	294.9
ISMBC	0.124	3.93×10^{-3}	1.92×10^{-2}	1.69	286.9
BC	0.374	3.11×10^{-2}	9.10×10^{-2}	3.787	272.8

5.2.3. Control Performance with Varing Loads

Figure 8a–c show the different control errors of PID, ISMBC and BC with loads of 100, 200 and 300 kg, respectively. From Section 2.3.2., the main component of the unmatched disturbance is external disturbance, and load is the main source of external disturbance. The ESO1 can accurately estimate the unmatched disturbance with varying loads, to realize the compensation for the unmatched disturbance. The estimated values of unmatched disturbances with varying loads are shown in Figure 8d. Based on the simulation results, the three evaluation indexes M_e, μ_e and σ_e were obtained and listed in Table 3.
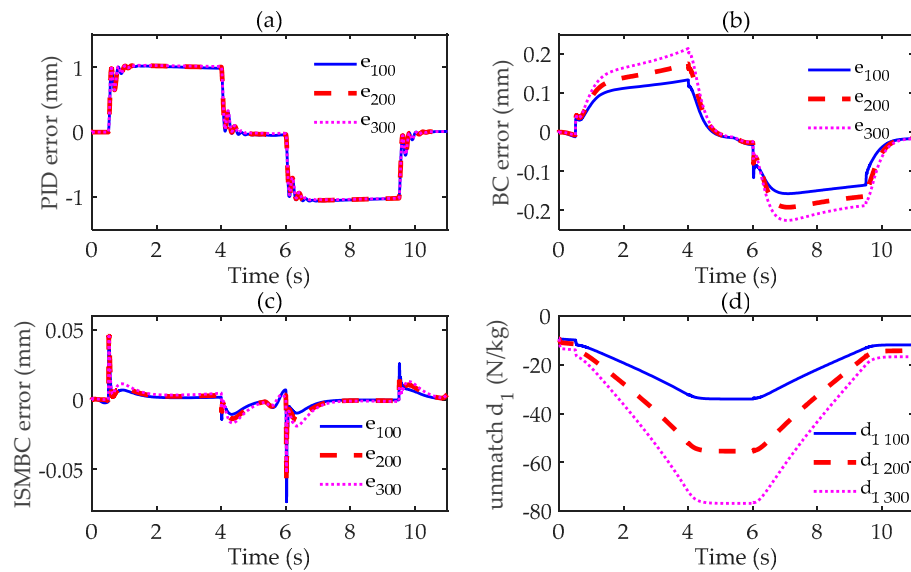
Figure 8. Position tracking error change of three controllers and external disturbance observation with varying loads: (**a**) position tracking errors of PID; (**b**) position tracking errors of BC; (**c**) position tracking errors of ISMBC; (**d**) estimation of external disturbances with varying loads.

From Table 3, it can be found that as the load increased, the indexes gradually decreased with the ISMBC controller. However, with the BC controller, only index μ_e showed a downward trend, and other indexes showed an upward trend. Thus, the results indicate that the integral sliding mode surface can enhance the robustness. In the meantime, only index M_e of the PID controller showed a downward trend, while other indexes showed an upward trend. It shows that within a certain range, larger load force can improve the control performance for the EHA.

Table 3. Comparison of the evaluation indexes of the three controllers with varying loads.

Controller	Load Mass [mm]	M_e [mm]	μ_e [mm]	σ_e [mm]
PID	100 kg	1.06	0.112	0.619
	200 kg	1.05	0.103	0.654
	300 kg	1.041	0.121	0.652
BC	100 kg	0.158	0.023	0.079
	200 kg	0.192	0.012	0.099
	300 kg	0.236	0.007	0.115
ISMBC	100 kg	0.073	0.003	0.013
	200 kg	0.061	0.003	0.012
	300 kg	0.052	0.001	0.011

5.2.4. Control Performance with Varying Disturbances

The swinging, the sudden increase and decrease in the load mass during motion, would also cause external disturbance. In order to simulate the swinging, a sine force $F_{sin} = 300\sin(2\pi t)$ was applied. On this basis, a pulse signal with an amplitude of 3000 N and a period of 2 s was added to simulate the sudden increase and decrease in the load. The simulation results are shown in Figure 9.
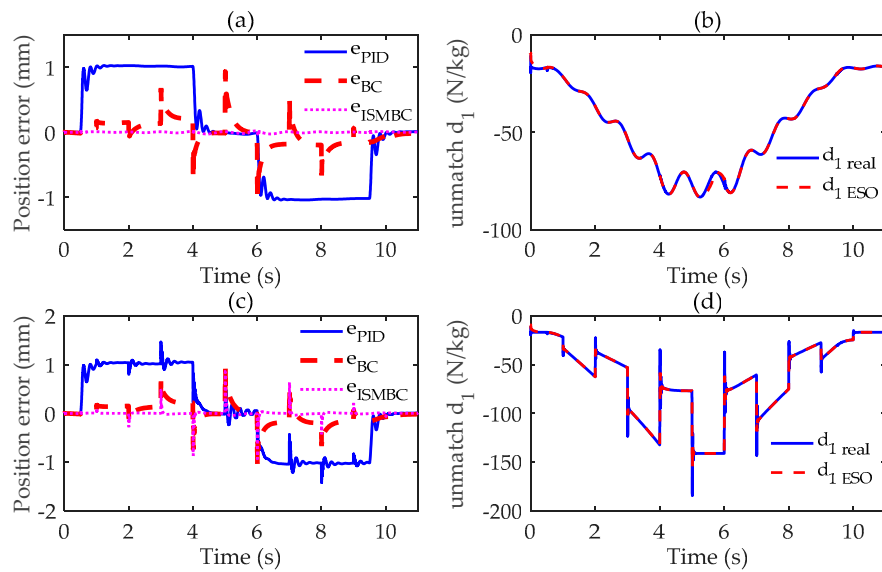
Figure 9. Simulation results of the three controllers with varying disturbances: (**a**) control errors with sine disturbance; (**b**) unmatching disturbance observed value with sine disturbance; (**c**) control errors with sine disturbance plus pulse disturbance; (**d**) unmatching disturbance observed value with sine disturbance plus pulse disturbance.

From Figure 9a,c, it can be seen that the ISMBC controller was the least affected, followed by the PID controller, and the BC controller was most affected by these external disturbances. This further proves that the integral sliding mode control has stronger anti-disturbance ability.

In summary, compared with the PID controller, the backstepping design can obtain higher control accuracy. In the first step of the backstepping design, the integral sliding mode surface is introduced into the position error term, which not only further improves the control accuracy but also boots the robustness.

6. Conclusions

This paper developed a novel control algorithm ISMBC that introduced integral sliding mode control into backstepping design, based on two extended state observers. The proposed control strategy was applied to solve the problems including nonlinearities, parameter uncertainties and external disturbances in the EHA. Lyapunov analysis showed that the proposed control system has higher stability and better robustness than the traditional backstepping design. A multi-domain model was established in the MATLAB/Simulink, including electric motor, hydraulic system, mechanism of a micro-crane and the proposed ISMBC controller. The following conclusions were obtained by simulation and analysis.

(1) Without load, the ISMBC controller showed the best control accuracy and fastest response. Compared with PID, the control accuracy can be increased by 89% and compared with backstepping control by 67%.

(2) With the loads of 100, 200 and 300 kg, the simulation results show that all control evaluation indexes of the ISMBC controller had a downward trend when load increased. With PID control, only the control accuracy index decreased slightly, and the other indexes showed an overall upward trend. However, all indexes of the BC controller increased.

(3) With load, sinusoidal force disturbance plus step force disturbance signals were applied to the system. The simulation results reveal that the ISMBC had the smallest position error and needed the least time to return to a stable state; the BC control had the largest error, but the oscillation during the recovery process was smaller than PID control.

The results of this study indicate that, compared with the PID controller, the BC controller can greatly improve the control accuracy of the system, but the system stability and robustness degrade. Hence, the ISMBC was proposed, by introducing the integral sliding mode control into the backstepping design. The simulation results show that the proposed ISMBC can not only further improve the control accuracy but also enhance system stability and robustness.

Although the ISMBC control algorithm can improve the control performance of the EHA, it has only been verified by simulation, without being verified by experiment. In the next stage of work, the test platform will be established for further proof and application. On the other hand, the proposed controller relies on accurate system parameters. In the following research, we will use adaptive law to estimate system parameters and to realize adaptive control.

Author Contributions: Conceptualization, S.Z., S.L. and F.D.; methodology, S.Z. and S.L.; software, S.L.; investigation, S.Z. and S.L.; writing—original draft preparation, S.Z. and S.L.; writing—review and editing, F.D.; supervision, S.Z.; project administration, F.D.; funding acquisition, F.D. All authors have read and agreed to the published version of the manuscript.

Conflicts of Interest: The authors declare no conflict of interest.

Abbreviations

The following abbreviations are used in this manuscript:

ISMBC	Integral Sliding Mode Backstepping Control
EHA	Electro-Hydrostatic Actuator
ESO	Extended State Observer
BC	Backstepping Control
PID	Proportional-Integral-Derivative

References

1. LI, Z.; Shang, Y.; Jiao, Z.; Lin, Y.; Wu, S.; LI, X. Analysis of the dynamic performance of an electro-hydrostatic actuator and improvement methods. *Chin. J. Aeronaut.* **2018**, *31*, 2312–2320.

2. Kuboth, S.; Heberle, F.; Weith, T.; Welzl, M.; König-Haagen, A.; Brüggemann, D. Experimental short-term investigation of model predictive heat pump control in residential buildings. *Energy Build.* **2019**, *204*, 109444.

3. Lin, T.; Lin, Y.; Ren, H.; Chen, H.; Chen, Q.; Li, Z. Development and key technologies of pure electric construction machinery. *Renew. Sustain. Energy Rev.* **2020**, *132*, 110080.

4. Li, K.; Lv, Z.; Lu, K.; Yu, P. Thermal-hydraulic Modeling and Simulation of the Hydraulic System based on the Electro-hydrostatic Actuator. *Procedia Eng.* **2014**, *80*, 272–281.

5. Quan, Z.; Quan, L.; Zhang, J. Review of energy efficient direct pump controlled cylinder electro-hydraulic technology. *Renew. Sustain. Energy Rev.* **2014**, *35*, 336–346.

6. Ge, L.; Quan, L.; Zhang, X.; Zhao, B.; Yang, J. Efficiency improvement and evaluation of electric hydraulic excavator with speed and displacement variable pump. *Energy Convers. Manag.* **2017**, *150*, 62–71.

7. Fu, S.; Wang, L.; Lin, T. Control of electric drive powertrain based on variable speed control in construction machinery. *Automat. Constr.* **2020**, *119*, 103281.

8. Navatha, A.; Bellad, K.; Hiremath, S.S.; Karunanidhi, S. Dynamic Analysis of Electro Hydrostatic Actuation System. *Procedia Technol.* **2016**, *25*, 1289–1296.

9. Ur Rehman, W.; Wang, S.; Wang, X.; Fan, L.; Shah, K.A. Motion synchronization in a dual redundant HA/EHA system by using a hybrid integrated intelligent control design. *Chin. J. Aeronaut.* **2016**, *29*, 789–798.

10. Xu, Z.; Liu, Y.; Hua, L.; Zhao, X.; Wang, X. Energy improvement of fineblanking press by valve-pump combined controlled hydraulic system with multiple accumulators. *J. Clean. Prod.* **2020**, *257*, 120505.

11. Kumar, M. A survey on electro hydrostatic actuator: Architecture and way ahead. *Mater. Today Proc.* **2020**, doi:10.1016/j.matpr.2020.10.049.

12. Altare, G.; Vacca, A. A Design Solution for Efficient and Compact Electro-hydraulic Actuators. *Procedia Eng.* **2015**, *106*, 8–16.

13. Mu, T.; Zhang, R.; Xu, H.; Zheng, Y.; Fei, Z.; Li, J. Study on improvement of hydraulic performance and internal flow pattern of the axial flow pump by groove flow control technology. *Renew. Energy* **2020**, *160*, 756–769.

14. Lyu, L.; Chen, Z.; Yao, B. Development of parallel-connected pump—Valve-coordinated control unit with improved performance and efficiency. *Mechatronics* **2020**, *70*, 102419.

15. Agostini, T.; De Negri, V.; Minav, T.; Pietola, M. Effect of Energy Recovery on Efficiency in Electro-Hydrostatic Closed System for Differential Actuator. *Actuators* **2020**, *9*, 12.

16. Gao, B.; Li, X.; Zeng, X.; Chen, H. Nonlinear control of direct-drive pump-controlled clutch actuator in consideration of pump efficiency map. *Control. Eng. Pract.* **2019**, *91*, 104110.

17. Ma, X.; Gao, D.; Liang, D. Improved Control Strategy of Variable Speed Pumps in Complex Chilled Water Systems Involving Plate Heat Exchangers. *Procedia Eng.* **2017**, *205*, 2800–2806.

18. Sakaino, S.; Tsuji, T. Resonance Suppression of Electro-hydrostatic Actuator by Full State Feedback Controller Using Load-side Information and Relative Velocity. *IFAC-PapersOnLine* **2017**, *50*, 12065–12070.

19. Sahu, G.N.; Singh, S.; Singh, A.; Law, M. Static and Dynamic Characterization and Control of a High-Performance Electro-Hydraulic Actuator. *Actuators* **2020**, *9*, 46.

20. Ohrem, S.J.; Holden, C. Modeling and Nonlinear Model Predictive Control of a Subsea Pump Station This work was carried out as a part of SUBPRO, a Research-based Innovation Centre within Subsea Production and Processing. The authors gratefully acknowledge the financial support from SUBPRO, which is financed by the Research Council of Norway, major industry partners, and NTNU. *IFAC-PapersOnLine* **2017**, *50*, 121–126.

21. Wei, S.G.; Zhao, S.D.; Zheng, J.M.; Zhang, Y. Self-tuning dead-zone compensation fuzzy logic controller for a switched-reluctance-motor direct-drive hydraulic press. *Proc. Inst. Mech. Eng. Part I J. Syst. Control Eng.* **2009**, *223*, 647–656.

22. Yan, L.; Qiao, H.; Jiao, Z.; Duan, Z.; Wang, T.; Chen, R. Linear motor tracking control based on adaptive robust control and extended state observer. In Proceedings of the 2017 IEEE International Conference on Cybernetics and Intelligent Systems (CIS) and IEEE Conference on Robotics, Automation and Mechatronics (RAM), Ningbo, China, 19–21 November 2017; pp. 704–709.

23. Cai, Y.; Ren, G.; Song, J.; Sepehri, N. High precision position control of electro-hydrostatic actuators in the presence of parametric uncertainties and uncertain nonlinearities. *Mechatronics* **2020**, *68*, 102363.

24. Lin, Y.; Shi, Y.; Burton, R. Modeling and Robust Discrete-Time Sliding-Mode Control Design for a Fluid Power Electrohydraulic Actuator (EHA) System. *IEEE/ASME Trans. Mechatron.* **2013**, *18*, 1–10.

25. Fu, M.; Liu, T.; Liu, J.; Gao, S. Neural network-based adaptive fast terminal sliding mode control for a class of SISO uncertain nonlinear systems. In Proceedings of the 2016 IEEE International Conference on Mechatronics and Automation, Harbin, China, 7–10 August 2016; pp. 1456–1460.

26. Alemu, A.E.; Fu, Y. In Sliding mode control of electro-hydrostatic actuator based on extended state observer. In Proceedings of the 2017 29th Chinese Control and Decision Conference (CCDC), Chongqing, China, 28–30 May 2017; pp. 758–763.

27. Sun, C.; Fang, J.; Wei, J.; Hu, B. Nonlinear Motion Control of a Hydraulic Press Based on an Extended Disturbance Observer. *IEEE Access* **2018**, *6*, 18502–18510.

28. WANG, Y.; GUO, S.; DONG, H. Modeling and control of a novel electro-hydrostatic actuator with adaptive pump displacement. *Chin. J. Aeronaut.* **2020**, *33*, 365–371.

29. Yang, G.; Yao, J. High-precision motion servo control of double-rod electro-hydraulic actuators with exact tracking performance. *ISA Trans.* **2020**, *103*, 266–279.

30. Shen, Y.; Wang, X.; Wang, S.; Mattila, J. An Adaptive Control Method for Electro-hydrostatic Actuator Based on Virtual Decomposition Control. In Proceedings of the 2020 Asia-Pacific International Symposium on Advanced Reliability and Maintenance Modeling (APARM), Vancouver, BC, Canada, 20–23 August 2020; pp. 1–6.

31. Yang, G.; Yao, J. Output feedback control of electro-hydraulic servo actuators with matched and mismatched disturbances rejection. *J. Frankl. Inst.* **2019**, *356*, 9152–9179.

32. Ren, G.; Costa, G.K.; Sepehri, N. Position control of an electro-hydrostatic asymmetric actuator operating in all quadrants. *Mechatronics* **2020**, *67*, 102344.

33. Jing, C.; Xu, H.; Jiang, J. Dynamic surface disturbance rejection control for electro-hydraulic load simulator. *Mech. Syst. Signal Process.* **2019**, *134*, 106293.

Publisher's Note: MDPI stays neutral with regard to jurisdictional claims in published maps and institutional affiliations.